Nano Energy 30 (2016) 450–459

Contents lists available at ScienceDirect

Nano Energy

journal homepage: www.elsevier.com/locate/nanoen

Self-powered liquid triboelectric microfluidic sensor for pressure sensing and finger motion monitoring applications

Qiongfeng Shi[a,b,c], Hao Wang[a,b,c], Tao Wang[a,b,c], Chengkuo Lee[a,b,c,d,*]

[a] Department of Electrical & Computer Engineering, National University of Singapore, 4 Engineering Drive 3, Singapore 117576, Singapore
[b] Center for Sensors and MEMS, National University of Singapore, 4 Engineering Drive 3, Singapore 117576, Singapore
[c] NUS Suzhou Research Institute (NUSRI), Suzhou Industrial Park, Suzhou 215123, PR China
[d] NUS Graduate School for Integrative Science and Engineering, National University of Singapore, Singapore 117456, Singapore

ARTICLE INFO

Keywords:
Self-powered
Liquid triboelectric
Capacitive
Microfluidic
Pressure sensor
Finger motion

ABSTRACT

Pressure sensors with flexibility are important functional components as the interface between the mechanical motion and electric signal in healthcare monitoring system. Conventional triboelectric based pressure sensors have advantages of simple structure configuration and self-powered sensing mechanism. However, the contact-separation working principle requires macro-scale air gap and the performance is largely affected by the separation distance, which is not suitable for conformal human motion sensing. Hence in this paper, we report a flexible microfluidic pressure sensor based on liquid-solid interface triboelectrification when liquid flows in a microfluidic channel. The proposed microfluidic pressure sensor is able to have a conformal contact with human skin and no separation gap is required due to the microfluidic chamber and channel design. It is capable of working in two sensing mechanisms – triboelectric mechanism and capacitive mechanism. Triboelectric mechanism can be used to detect the dynamic pressure change on device without external power supply. Capacitive mechanism can be adopted as complementary sensing mechanism to detect both dynamic pressure change and static pressure. The proposed microfluidic pressure sensor can monitor both the magnitude and frequency of the pressure applied on the device simultaneously. Besides, the device can be integrated with microfluidic system as a self-powered flow rate sensor. Moreover, it can be conformally attached on human finger for finger bending degree and bending frequency detection. The proposed microfluidic pressure sensor offers more usage flexibility for flow rate, finger motion monitoring and the potentials for more complex human motion monitoring applications.

1. Introduction

Diversified flexible and wearable sensors are developing rapidly across the world in healthcare monitoring system, including implantable biomedical sensors [1], mechanoreceptors [2], tactile sensors [3–5], pressure sensors [6–8], etc. Among these research effort, pressure sensor is a critical functional component which acts as the interface between the mechanical motion and electric signal. Flexible and wearable pressure sensors are of high interest because of their diversified applications in healthcare monitoring system, such as electronic skin [9–12], blood pressure monitoring [13] and pulse waveform monitoring [14,15]. In human-machine interface and game control, flexible and wearable pressure sensors are also developing quickly and considered as important components in the applications like soft robotics [16,17] and gesture recognition [18–20]. Currently, most pressure sensors are based on the mechanism of force-induced change in one typical parameter, e.g. resistance [21–24], capacitance [25–28], piezoelectric output [29–32], or triboelectric output [33–36]. For resistive and capacitive mechanism, they normally require external power supply to facilitate the pressure sensing. In many practical applications like implantable pressure sensors, periodical replacement of the batteries may cause severe health risks to patients. Therefore, it is important for the pressure sensor in these systems to be self-powered, wireless, and maintenance-free.

To enable self-powered pressure sensing, piezoelectric or triboelectric mechanism can be adopted. Working principle of piezoelectric mechanism is based on the well-known piezoelectric effect. When different force-induced strain is created on the piezoelectric material, different piezopotentials will be generated in the material according to d_{31} or d_{33} design [37,38]. Traditional piezoelectric PZT and AlN based pressure sensors are not compatible with flexible substrates due to the high fabrication temperature. Although new fabrication process or new

* Corresponding author at: Department of Electrical & Computer Engineering, National University of Singapore, 4 Engineering Drive 3, Singapore 117576, Singapore.
E-mail address: elelc@nus.edu.sg (C. Lee).

http://dx.doi.org/10.1016/j.nanoen.2016.10.046
Received 6 September 2016; Received in revised form 15 October 2016; Accepted 20 October 2016
Available online 24 October 2016
2211-2855/

piezoelectric materials like PVDF can be introduced to realize the flexible pressure sensors, the process is still too complicated and not cost-effective [30–32]. Triboelectric mechanism is based on the triboelectrification or contact electrification between two materials with different electron affiliation. When the two materials come into contact, one material tends to attract electrons thus becoming negatively charged, while the other material tends to lose electrons resulting in positively charged. When they are separated, the positive and negative charge will induce potential difference, driving electrons to flow in the external circuit. Triboelectric based pressure sensors have simple structure configuration that is cost-effective even for large area sensing and can be easily fabricated on various flexible substrates at low temperature. Triboelectric based nanogenerators and self-powered sensors have been rapidly developed in the past few years [33–36,39–47]. Wang et al. reviewed the triboelectric nanogenerators progress and their applications as self-powered sensors for different usage scenarios [48]. Recent development of triboelectric nanogenerators as wireless self-powered sensors was reviewed by Wang et al. [49]. These simple structure configuration triboelectric sensors enable self-powered sensing and are used for various applications such as pressure change, physical touching and acceleration detection, etc.

However, conventional triboelectric based pressure sensors work on the vertical contact-separation mode which requires a macro-scale air gap and the performance is largely affected by the separation distance [33–36]. For the application of human motion sensing, pressure sensors need to be attached on human skin, fingers, and elbow joints, etc. Devices should have conformal contact with skin in which macro-scale separation is difficult to achieve. Conventional triboelectric based pressure sensors may not work properly under these circumstances. Liquid integrated with soft substrates can have high flexibility and provide conformal contact with different curvy surfaces because of the amorphous nature of liquid. Yeo et al. proposed a graphene oxide nanosuspension liquid-based resistive microfluidic tactile sensor with superior mechanical flexibility and conformability [50] and a flexible thin film resistive microfluidic tactile sensor based on highly conductive metallic liquid – eutectic gallium indium [51]. But the resistive sensing mechanism requires external power supply which is not suitable for self-powered applications. Lately, liquid-solid interface triboelectric based generators are developed for energy harvesting and self-powered sensing [52–65]. Liquid as positive triboelectric material can provide proper contact and thus enlarge the total contact area. Different applications based on liquid triboelectric generators have been demonstrated by many researchers. Lin et al. firstly demonstrated a triboelectric generator based on conformal water–solid surface contact electrification [52]. Jeon et al. reported a triboelectric 3-dimensional broadband energy harvester based on the oscillation of encapsulated liquid and a self-powered NaCl ion concentration sensor on rigid Si substrate based on liquid–solid contact triboelectrification [53,54]. Li et al. proposed a self-powered triboelectric nanosensor for microfluidic flow rate sensing application [55]. To date, there is no study reported about self-powered pressure sensing based on liquid-solid interface triboelectrification. If a liquid-solid interface triboelectric sensor integrated with microfluidic channel and chamber can be realized on flexible substrate, it can then function as a self-powered conformal pressure sensor. When different pressure is applied on the chamber filled with liquid, different volume of liquid will flow in the channel and thus different output signals will be generated.

Here, we report a microfluidic pressure/force sensor (pressure P can be calculated from force F and contact area S by $P = F/S$) that is able to work on two sensing mechanisms – self-powered triboelectric mechanism and capacitive mechanism, and we also study the sensitivity and linear sensing range of these two mechanisms. For most proposed pressure sensors working on one sensing mechanism, comparison between different sensing mechanisms is not quite fair since device structure is different. In this paper, we use the same device to provide a fair comparison between triboelectric mechanism and capacitive mechanism based on sensitivity and linear sensing range. Triboelectric sensing mechanism is a self-powered sensing mechanism which is suitable for wireless sensing. It has better sensitivity and larger linear sensing range compared to capacitive sensing mechanism. However, it can only be used for dynamic pressure sensing. This is because triboelectric mechanism requires liquid to flow across the electrode in order to generate output signal. When there is no change of pressure to induce movement of liquid front (interface of liquid and air) along the channel, there will be no triboelectric output, which is the same as 0 pressure. Although capacitive sensing mechanism is not self-powered, it can measure both the dynamic pressure and the static pressure. When a pressure is applied on the device, there will be liquid in the channel no matter whether the pressure is applied in a dynamic or static manner. Different liquid front position will result in different capacitance change even when it is not moving. Therefore, capacitive sensing mechanism can be adopted as a complementary sensing mechanism to determine the magnitude of a static pressure. We can choose triboelectric mechanism for self-powered dynamic pressure sensing and choose capacitive mechanism for complementary static pressure sensing. The proposed microfluidic pressure sensor is able to simultaneously monitor both the magnitude and frequency of the pressure applied on the device. With the multiple electrodes design, it can also be integrated with microfluidic system as a self-powered flow rate sensor. Moreover, we successfully demonstrated that the proposed microfluidic pressure sensor can be conformally attached on human finger to monitor finger bending degree and bending frequency.

2. Experiment

2.1. Device structure and working principle of the microfluidic pressure sensor

Schematic drawing of the proposed microfluidic pressure sensor attached on the index finger for finger motion monitoring is shown in Fig. 1(a). Device structure of tilted view and cross-sectional view is illustrated in Fig. 1(b). The microfluidic pressure sensor consists of flexible polyethylene terephthalate (PET) substrate, multiple Cu electrodes, thin polydimethylsiloxane (PDMS) layer as triboelectric layer, PDMS structure layer with microfluidic channel and chamber, and small PDMS disc to effectively transfer the applied pressure to the chamber. One chamber of the microfluidic pressure sensor is filled with de-ionized (DI) water and the other chamber is filled with air. E1 to E6 in top part of Fig. 1(b) denotes the 6 Cu electrodes from the water chamber all along to the air chamber. Top view photograph of the device and tilted view photograph of the device bended by hand are shown in Fig. 1(c). When the microfluidic pressure sensor is fixed on a human finger, the center of the water chamber is facing the finger joint. When finger bends to different degrees, different pressure due to the bending motion will be applied on the water chamber and thus induces water flow in the channel. Then different triboelectric output and capacitive output can be measured from the multiple Cu electrodes underneath the channel.

Fabrication process of the microfluidic pressure sensor is depicted by Fig. S1 in the Supplementary information. For the fabrication of bottom part, flexible PET substrate is first cut into a 3.5 cm × 11 cm rectangular shape. Then the multiple Cu tape electrodes are attached on the PET substrate. After that, a thin PDMS layer is spin-coated on top of the Cu electrodes at 1000 rpm for 60 s. The PDMS layer is cured at 75 °C for 30 min. For the top part of the device, SU-8 photoresist is spin-coated and patterned on Si substrate by photolithography. Then PDMS is casting on the SU-8 mould and cured for overnight. After that, the PDMS layer is carefully peeled off from the SU-8 mould. A thin PDMS film is cut into circular disc shape as the effective pressure transfer element. All these three parts are bonded together by using O_2 plasma treatment. Lastly, DI water is injected into one chamber by syringe needle. Fig. S2 in the Supplementary information shows the

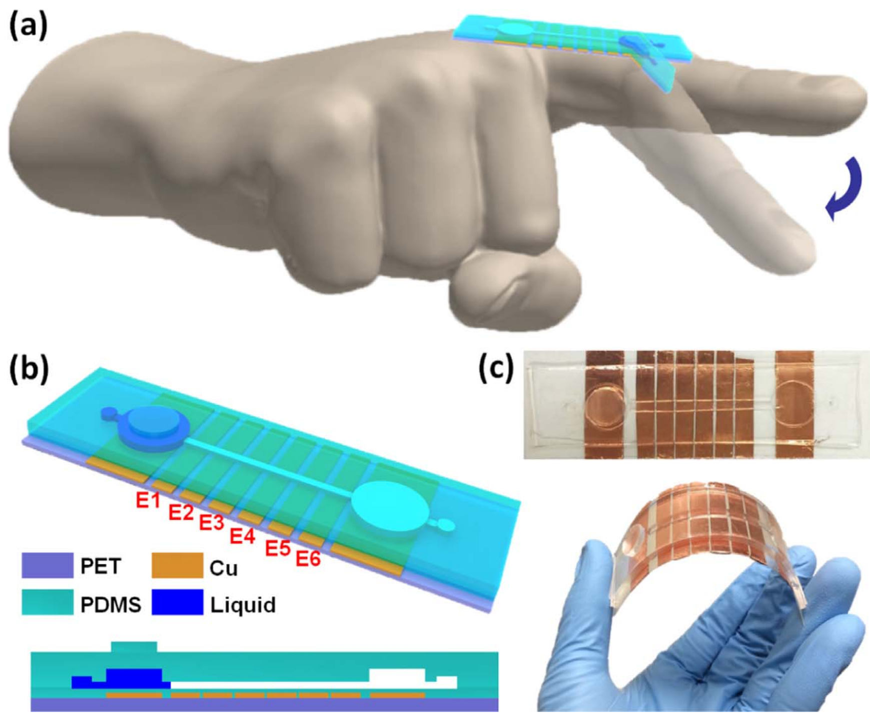

Fig. 1. (a) Schematic drawing of the proposed microfluidic pressure sensor attached on the index finger for finger motion monitoring application. (b) Device structure and cross-sectional view of the proposed microfluidic pressure sensor. (c) Top view photograph of the device and tilted view photograph of the device when bended by hand.

optical microscope image and scanning electron microscope (SEM) image of the microfluidic channel.

The working principle of triboelectric mechanism is based on the triboelectrification between water and PDMS layer and electrostatic induction. For single electrode mode, as illustrated in Fig. 2(a), when water first comes into contact with PDMS channel and separates, PDMS attracts electrons from water. Thus PDMS layer ends with negatively charged and water with positively charged due to different electron affiliation. The initial state is water with positive charges in chamber, PDMS with negative charges and Cu electrodes with positive charges to balance the electrical potential. When a certain pressure is applied on the water chamber, the chamber is compressed and water flows into the channel. Once water front (interface of water and air) is flowing across the Cu electrode, the positive charges in water will balance the negative charges on the PDMS layer, thus electrons are forced to flow from ground to Cu electrode. When pressure is released and water flows back to chamber, then the negative charges on PDMS layer force electrons to flow to ground. Therefore, for single electrode mode, there is a positive peak when water front flows forward across the Cu electrode and a negative peak when water front flows backward. For interdigital (IDT) electrode mode, it can be considered as a few pairs of double electrode mode connected in parallel. The working principle of the double electrode mode is shown in Fig. 2(b), which is similar as the single electrode mode. The difference is that in the double electron mode, electrons flow between two Cu electrodes instead of flowing between the Cu electrode and the ground. At the

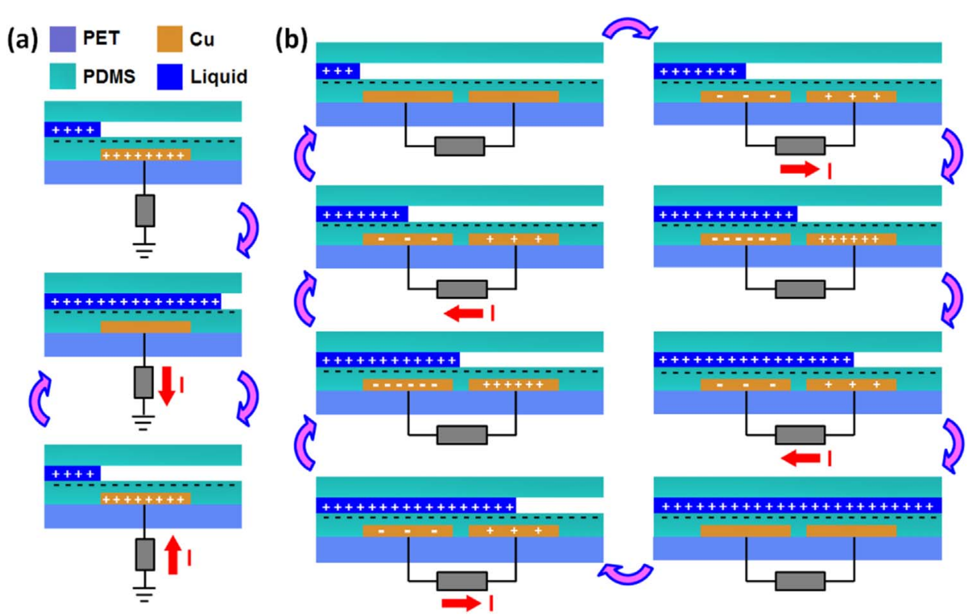

Fig. 2. Working principle of triboelectric mechanism under (a) single electrode mode and (b) IDT electrode mode.

initial state when the channel is already wetted by water once, water is positively charged and PDMS layer is negatively charged. When a pressure is applied on the water chamber, the chamber is compressed and water flows into the channel. Once the water front is across the first Cu electrode, the positive charges in water will induce potential difference between the two Cu electrodes, thus electrons are forced to flow from the second Cu electrode to the first Cu electrode. When water front is moving through the gap between the first and the second Cu electrode, then there is no current. When water continues to flow forward across the second Cu electrode, electrons flow from the first Cu electrode back to the second Cu electrode due to potential difference is reduced. Once water front leaves the second Cu electrode, no current is generated. When the pressure is released and water flows backward to chamber, electrons firstly flow from the second Cu electrode to the first Cu electrode and then flow in a reversed direction due to the potential difference of the two Cu electrodes.

3. Result and discussion

3.1. Self-powered triboelectric single electrode mode for pressure and flow rate sensing

Testing setup for single electrode triboelectric output measurement is depicted in Fig. 3(a). Ammeter or Oscilloscope is connected to electrode 1 (E1) for triboelectric current and voltage measurement. First we use finger to periodically press and release the water chamber to activate water to flow forward and backward in the channel. Waveform of output current and voltage from E1 is shown in Fig. S3(a) and (b) in Supplementary information, respectively. Peak to peak current (Ipp) is ~12 nA and peak to peak voltage (Vpp) is ~19 mV.

In order to accurately study the dependence of output performance with the magnitude and frequency of the applied pressure, a force gauge testing system is used to generate force upon the water chamber. The force gauge testing system is mainly composed of a fixed platform and a moving stage. The device is attached on the fixed platform with water chamber in the center. Distance between moving stage and fixed platform, force magnitude and moving speed of the moving stage can be pre-set. Then the moving stage moves towards the device in the pre-set speed (100 mm/min to 900 mm/min) until force reaches the pre-set magnitude. Once force reaches the pre-set magnitude, the moving stage then moves apart from the device with the same speed to the original position and begins next cycle.

The relationship of Ipp from E1 and input force magnitude is shown in Fig. 3(d) when the stage moving speed is fixed at 500 mm/min. It can be seen that Ipp of E1 linearly increases with applied force. When applied force is 0.4 N, Ipp of E1 is 1.19 nA as shown in Fig. 3(e). When applied force increases to 11.6 N, Ipp increases to 1.62 nA as depicted in Fig. 3(f). Sensitivity of force sensing is 0.0323 N^{-1} based on the following Equation

$$S = \frac{d(\Delta I/I)}{d\Delta F} \tag{1}$$

where S is the sensitivity, ΔI is current increment and I is the original current when force magnitude of F is applied, and ΔF is the force

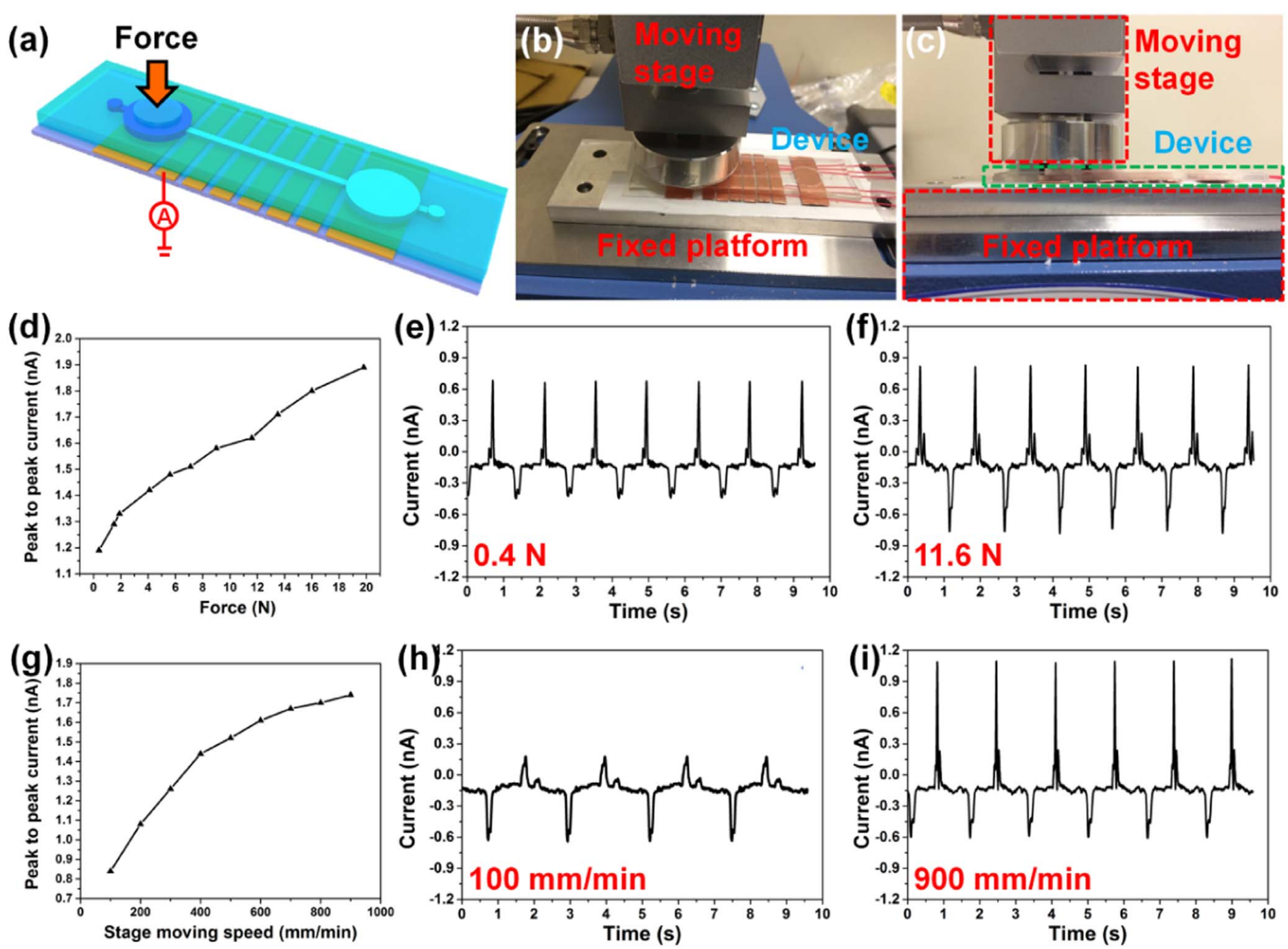

Fig. 3. (a) Testing setup for triboelectric single electrode mode sensing. (b) Tilted view and (c) side view of the device tested by a force gauge testing system. (d) Relationship of output peak to peak current and the applied force. Output current waveform when applied force is (e) 0.4 N and (f) 11.6 N. (d) Relationship of output peak to peak current and the applied stage moving speed. Output current waveform when applied stage moving speed is (e) 100 mm/min and (f) 900 mm/min.

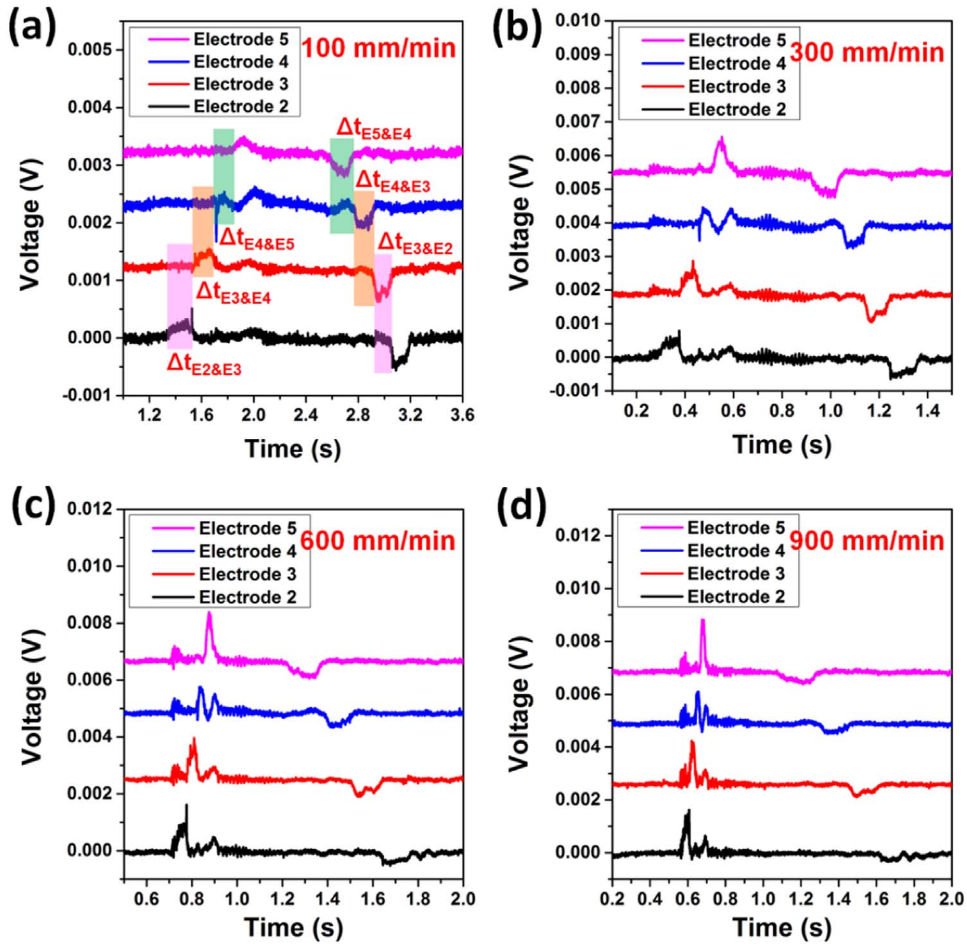

Fig. 4. Flow rate measurement based on triboelectric single electrode mode. Output voltage waveform of Electrode 2, 3, 4 and 5 when stage moving speed is (a) 100 mm/min, (b) 300 mm/min, (c) 600 mm/min and (d) 900 mm/min.

Table 1
Time difference between two adjacent electrodes for forward flowing and backward flowing of water.

Speed	Forward flowing time difference (ms)			Backward flowing time difference (ms)		
	$\Delta t_{E2\,\&\,E3}$	$\Delta t_{E3\,\&\,E4}$	$\Delta t_{E4\,\&\,E5}$	$\Delta t_{E5\,\&\,E4}$	$\Delta t_{E4\,\&\,E3}$	$\Delta t_{E3\,\&\,E2}$
100 mm/min	160	130	130	140	130	120
300 mm/min	50	60	60	100	100	130
600 mm/min	38	38	32	140	130	140
900 mm/min	28	28	20	140	160	160

increment. The increment of Ipp from E1 with increasing applied force is due to two reasons. Firstly, higher force on the water chamber deforms the chamber more, and then more volume of water will be squeezed into the channel simultaneously. Hence forward flow rate of water front with higher force is larger and thus positive peak of Ipp is higher. Secondly, when more water is squeezed into the channel due to higher force, the air pressure in the air chamber is higher. Once the applied force is released, water needs to flow back due to the unbalanced high air pressure in the air chamber. The higher air pressure generates higher backward flow rate of water front and thus higher negative peak of Ipp. Therefore, the overall Ipp of E1 increases when the applied force on water chamber increases. In the future, the output performance of the microfluidic sensor can be further improved by having micro/nano structures in the microfluidic channel and adding high dielectric constant material to the PDMS layer, etc.

Fig. 3(g) shows the relationship of Ipp from E1 and the stage moving speed when the applied force is fixed at 10 N. It can be observed from the relationship curve that Ipp of E1 also linearly increases with the speed of the moving stage. When applied speed increases from 100 mm/min to 900 mm/min, Ipp of E1 increases from 0.84 to 1.74 nA. The major reason responsible for the increment of Ipp from E1 with increasing applied speed is the higher forward flow rate of water front. When higher stage moving speed is applied to the device, it means the frequency is higher. Although the volume of water being squeezed into the channel is the same, water needs to flow to the same position in a shorter time with higher stage moving speed. Thus forward flow rate is higher and positive peak of Ipp is higher. Since the air in the air chamber is always compressed to the same extend, the backward flow rate of water driven by the air pressure is the same. Therefore, the negative peak of Ipp is always the same. In summary, when higher magnitude of force is applied on the water chamber, both positive peak and negative peak of Ipp will increase. When higher frequency of force is applied, it mainly affects and improves the positive peak of Ipp.

Due to the advantage of the multiple electrodes design and self-powered sensing mechanism, the device can be integrated with microfluidic system for self-powered flow rate monitoring. When electrode 2, 3, 4 and 5 (E2, E3, E4 and E5) are connected to different channels of oscilloscope, the device can function as a self-powered flow rate sensor. Different flow rates are generated by setting different speed of the moving stage with same applied force of 10 N. It can be seen from Fig. 4(a)–(d) that when water flows across E2, E3, E4 and E5, positive peak of output current is generated consecutively on each electrode. When water flows back, negative peak appears on each electrode in a reverse order. By measuring the time difference of output

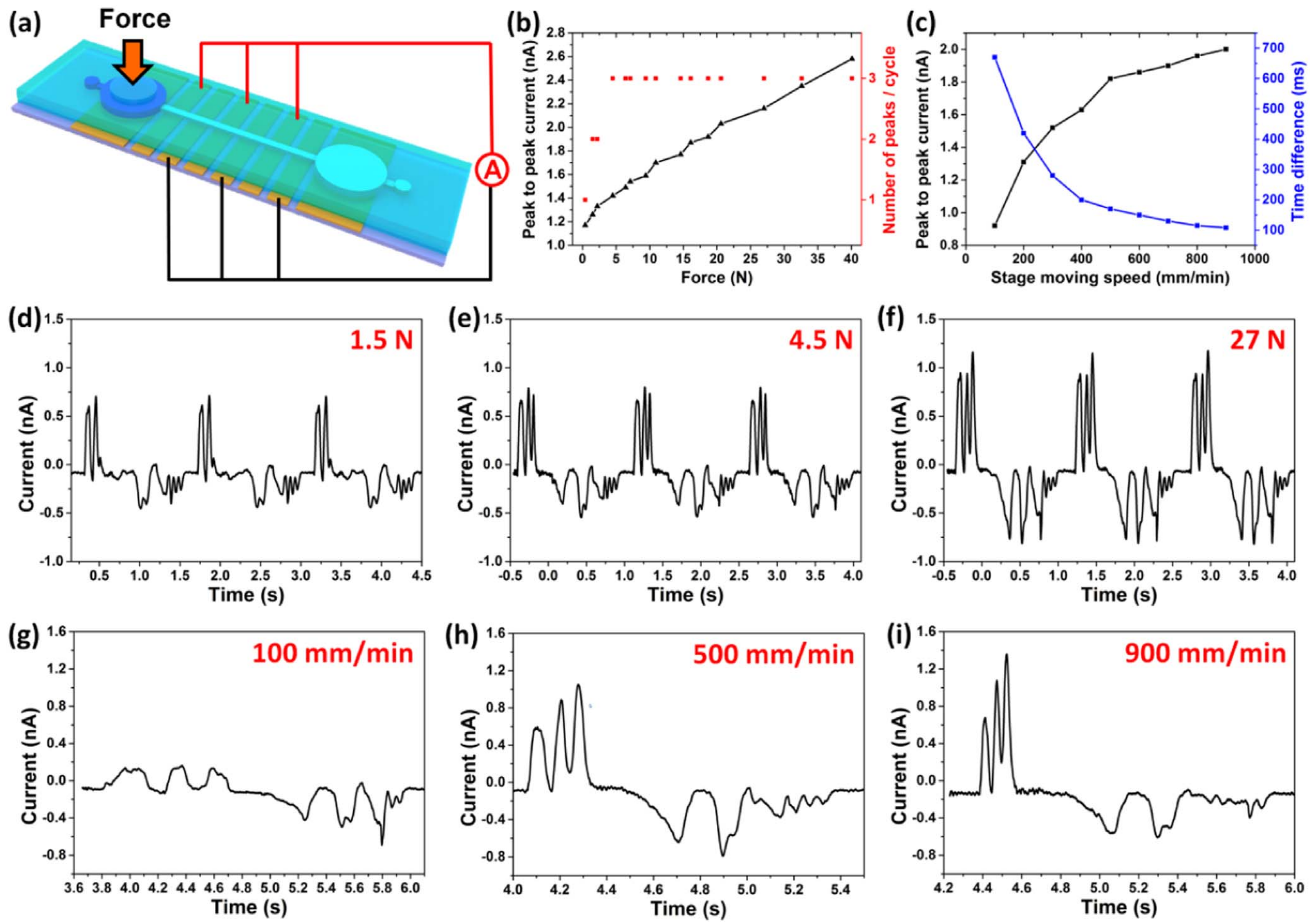

Fig. 5. (a) Testing setup for triboelectric IDT electrode mode sensing. (b) Relationship of output peak to peak current and the applied force. Number of peaks in each cycle is shown in another y axis. (c) Relationship of output peak to peak current and the applied stage moving speed. Time difference between water flowing from first pair to third pair IDT electrode is shown in another y axis. Output current waveform when applied force is (d) 1.5 N, (e) 4.5 N and (f) 27 N. Output current waveform when applied stage moving speed is (g) 100 mm/min, (h) 500 mm/min and (i) 900 mm/min.

signal and actual distance between either two electrodes, the average forward and backward flow rate between the two electrodes can be calculated. Time difference between two adjacent electrodes for forward flowing and backward flowing is summarized in Table 1. Since stage moving speed only affects the forward water flow rate, the time difference between two adjacent electrodes for forward water flowing decreases when stage moving speed increases while the time difference between two adjacent electrodes for backward water flowing keeps constant.

3.2. Self-powered triboelectric IDT electrode mode for pressure and flow rate sensing

By connecting the multiple Cu electrodes in single electrode mode, the device is able to function as a self-powered pressure sensor and flow rate sensor. But collecting signals from multiple measurement channels simultaneously may be limited by measurement equipment and increase the signal process complexity. Therefore, in order to overcome this problem, the multiple Cu electrodes are connected into IDT electrode to enable pressure and flow rate sensing by collecting signal from only one measurement channel, as depicted in Fig. 5(a). Fig. 5(b) shows the dependence of Ipp with the magnitude of applied force at the same stage moving speed of 500 mm/min. Sensitivity of force sensing with IDT electrode mode is 0.0304 N^{-1}. Detail current waveform with applied force of 1.5, 4.5 and 27 N is shown in Fig. 5(d)–(f), respectively. It can be seen from Fig. 5(b) that Ipp linearly increases with applied force. When applied force increases from 0.4 to 40 N, Ipp increases from 1.17 to 2.58 nA. The increment in both the positive and negative peak of Ipp is induced by higher forward and backward flow rate when higher force is applied. Number of peaks in each cycle of the current waveform with different applied force is also depicted in Fig. 5(b). It is worth to note that there is only one peak in each cycle of the current waveform when force is below 1 N. There are two peaks in the current waveform when force is between 1 and 3 N, while three peaks appear when force is above 3 N. This is because that when the applied force is below 1 N, water front can only reaches the first pair IDT electrode and thus only one peak appears. When force is between 1 and 3 N, water front can reach the second pair IDT electrode and hence two peaks are generated. When force is above 3 N, water front can reach the third pair IDT electrode, resulting in three peaks in each cycle. Number of peaks in each cycle can act as a rough estimation of force range while current magnitude can act as a fine estimation of force magnitude. Typical output voltage waveform from the IDT electrode is shown in Fig. S4 of the Supplementary information when it is tested by force gauge.

Fig. 5(c) shows the relationship of Ipp and stage moving speed when the applied force is fixed at 15 N. Detail current waveform with 100, 500 and 900 mm/min speed is shown in Fig. 5(g), (h) and (i), respectively. It can be observed that Ipp increases with speed of the moving stage. When applied speed increases from 100 mm/min to 900 mm/min, Ipp increases from 0.92 to 2 nA. The increment of Ipp with increasing stage moving speed is due to the higher forward flow rate of water. Benefited from the multiple peaks from the IDT electrode, we can use these peaks to measure the flow rate. Time

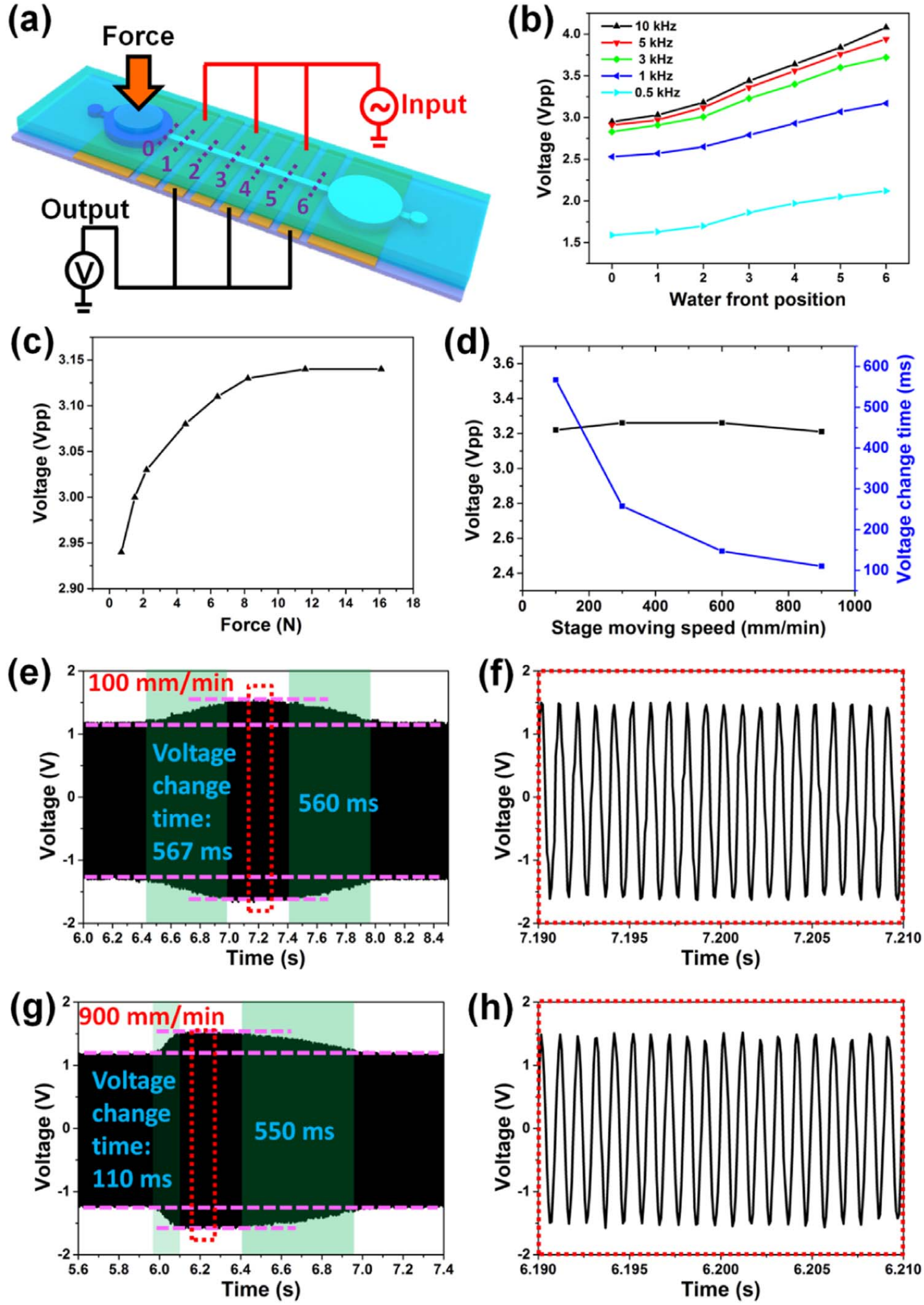

Fig. 6. (a) Testing setup for capacitive sensing. (b) Output voltage when water is in different position in the channel with different frequency of the applied sinusoidal wave. (c) Relationship of output voltage and the applied force. (d) Relationship of output voltage and the applied stage moving speed. Voltage change time from the original value to final value with different applied stage moving speed is shown in another y axis. (e) Output voltage waveform when applied stage moving speed is 100 mm/min. (f) Enlarged view of red dash rectangular voltage waveform in (e). (g) Output voltage waveform when applied stage moving speed is 900 mm/min. (h) Enlarged view of red dash rectangular voltage waveform in (g).

difference of positive peak from the first pair IDT electrode to the third pair IDT electrode is also plotted in Fig. 5(c). Time difference decreases when the stage moving speed increases. This is because when stage moving speed increases, forward flow rate in channel also increases and thus the time difference decreases. By measuring the time difference and actual distance between the first and the third pair IDT electrode, flow rate can be calculated accordingly. Therefore, by connecting the multiple Cu electrodes into IDT electrode, force sensing and flow rate sensing from only one measurement channel can be realized, providing potentials in more diversified applications.

3.3. Capacitive mechanism for pressure and flow rate sensing

Although triboelectric mechanism is self-powered, it requires the water to flow across the electrode to generate signals. When in a static state with no water flowing, triboelectric mechanism cannot determine the pressure or force magnitude. In this case, capacitive mechanism can be used as a complementary sensing mechanism since it can work under both dynamic and static state. The principle of capacitive mechanism is that when water is in the channel and covers two adjacent electrodes, the capacitance between these two electrodes is greatly increased due to the high dielectric constant of water compared to air. Hence for the IDT electrode, when water front is in different

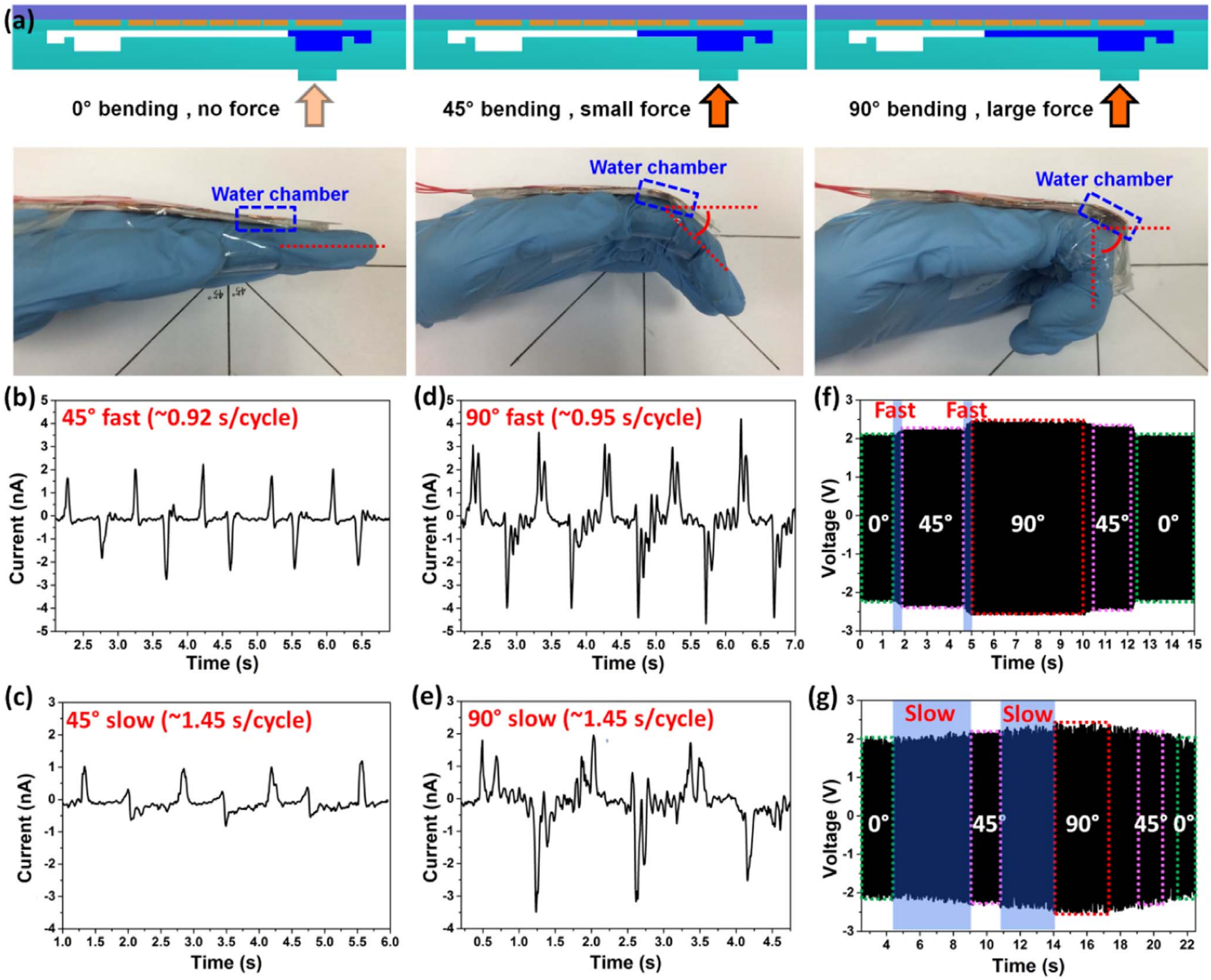

Fig. 7. Demonstration of the device functioned as a finger motion sensor. (a) From left to right is finger bending photograph with bending degree of 0°, 45° and 90°. Output current waveform from triboelectric IDT electrode mode when finger bending to 45° in a (b) fast and (c) slow manner. Output current waveform from triboelectric IDT electrode mode when finger bending to 90° in a (d) fast and (e) slow manner. Output voltage waveform from capacitive sensing when finger consecutive bending to 0°, 45°, 90°, 45° and 0° in a (f) fast and (g) slow manner.

positions in the channel due to different applied force, the overall capacitance of the IDT electrode is different. The speed or frequency of applied force affects the time difference from original capacitance to final capacitance but does not affect the value of final capacitance when applied force is the same. To facilitate the real-time measurement of capacitance change, we use the testing setup as shown in Fig. 6(a). The upper part of the IDT electrode is connected to a signal generator supplying sinusoidal signal with Vpp magnitude of 10 V and the lower part of the IDT electrode is connected to oscilloscope for voltage measurement. Since the major change of output voltage is when water covers two adjacent electrodes, we first measure the output voltage when water front is at different position along the channel. Water front position from 0 to 6 is defined as the middle line of each electrode and indicated in Fig. 6(a). By applying 5 different frequencies from 500 Hz to 10 kHz, output voltage of different water front position is plotted in Fig. 6(b). The water front reaches position 0–6 is realized by static force applied on the water chamber, indicating the capability of static pressure sensing by capacitive mechanism. Output voltage increases when water front reaches the position from 0 to 6 due to the increment in IDT electrode capacitance and thus decrement in IDT electrode impedance. Output voltage increases with increasing input source frequency, since the impedance of IDT electrode decreases when frequency increases.

Fig. 6(c) shows the maximum output voltage when different force is applied on the water chamber. The frequency and magnitude of sinusoidal signal is fixed at 1 kHz and Vpp magnitude of 10 V for the measurement. It can be observed that in lower force range (< 10 N), output voltage increases almost linearly with applied force. But in higher force range (> 10 N), output voltage increases very slowly and saturated soon. By comparing the force sensing measurement with triboelectric IDT electrode mode, capacitive mechanism has a lower sensitivity of 0.0086 N^{-1} and also a fast saturated force range. The fast saturated force range is due to the nature of capacitive sensing mechanism. Since capacitance change is only determined by the final position of water in the channel while flow rate of water has no influence on the final capacitance. For the applied force in the lower magnitude range (< 10 N), the water chamber is more compressible and water front position rapidly increases. For the applied force in the higher magnitude range (> 10 N), only a limited volume of water can be squeezed out of the water chamber because of the higher air pressure in the air chamber and water front position slowly increases and rapidly saturates. Instead, for triboelectric mechanism in the higher magnitude range (> 10 N), higher force generates higher forward flow rate and also higher backward flow rate which can be differentiated by the triboelectric current output. Thus triboelectric mechanism based on current magnitude shows better linear sensing range compared with the capacitive mechanism.

When different stage moving speed is applied, maximum output voltage and voltage change time from original state to final state is shown in Fig. 6(d). Detailed voltage waveform of 100 mm/min and 900 mm/min moving speed is plotted in Fig. 6(e) and (g). Fig. 6(f) and (h) are the zoom-in waveform of the red dash rectangle part of Fig. 6(e) and (g). Maximum output voltage of different stage moving speed is almost the same since applied force is the same of 15 N. But the flow rate of different stage moving speed is different and indicated by the voltage change time in Fig. 6(d). It can be seen that voltage change time decreases when flow rate increases. Thus by measuring the voltage change time in the voltage waveform and water position indicated by the maximum output voltage, flow rate of water in the channel can be calculated. Therefore, capacitive mechanism can be used for flow rate sensing, dynamic pressure sensing and static pressure sensing.

3.4. Demonstration of finger motion monitoring

To demonstrate the practical monitoring capability of the microfluidic pressure sensor, the device is fixed on a human finger and used as a finger motion sensor for bending degree and bending frequency monitoring. Fig. 7(a) from left to right indicates the device fixed on a human finger with 0°, 45° and 90° bending degree. The cross-sectional schematic drawing indicates the water front position in the channel with different bending degrees. Fig. 7(b)–(e) shows the triboelectric output current waveform from the IDT electrode when finger is bended to different degree in a fast or slow manner. When finger is periodically bended to 45° as in Fig. 7(b) and (c), current signal with one peak in each cycle is shown in the waveform. This is because the applied force on the water chamber when bending to 45° can only squeeze water to the first pair IDT electrode. When finger is bended to 90° as in Fig. 7(d) and (e), current signal with two peaks in each cycle appears since the applied force on the water chamber can squeeze water to the second pair IDT electrode. When the finger is bending at a fast manner, output current is higher due to a higher flow rate of water front. Capacitive sensing results are shown in Fig. 7(f) and (g) for fast bending manner and slow bending manner in consecutive bending degree of 0°, 45°, 90°, 45° and 0°. Bending degree can be observed from the output voltage magnitude and bending rate can be observed from the time difference between two bending degree in the signal waveform. For the future application, the device can be improved by adding more pairs of IDT electrode, enabling the detection of bending degree and finger motion with higher resolution.

4. Conclusion

In summary, we propose a microfluidic pressure sensor with two sensing mechanisms – triboelectric and capacitive mechanism, offering more flexibility for using in dynamic pressure sensing and static pressure sensing situation. Under triboelectric mechanism, it can work as a self-powered dynamic pressure sensor by using single electrode mode or IDT electrode mode. For capacitive mechanism, it can monitor the pressure applied on device in both dynamic and static state. The device is able to monitor both the magnitude and frequency of the applied pressure simultaneously. For force magnitude sensing, triboelectric mechanism shows better sensitivity and larger linear sensing range compared to capacitive mechanism. Because of the multiple electrode design, the device can be readily integrated with microfluidic system as self-powered flow rate sensor. The device can be conformally attached on human finger for bending degree and bending frequency monitoring. In the future, with further optimized multiple electrodes design, the microfluidic pressure sensor can be used for more complex finger motion monitoring and other human motion monitoring.

Acknowledgement

The authors acknowledge the financial support from the following research grants: Ministry of Education (MOE) Faculty Research Committee (FRC) Grant (R-263-000-B56-112) “Thermoelectric Power Generator (TEG) Based Self-Powered ECG Plaster – System Integration (Part 3)” at the National University of Singapore; NRF-CRP8-2011-01 Grant (R-263-000-A27-281) “Self-Powered Body Sensor Network for Disease Management and Prevention Oriented Healthcare” by the National Research Foundation (NRF), Singapore.

Appendix A. Supplementary material

Supplementary data associated with this article can be found in the online version at http://dx.doi.org/10.1016/j.nanoen.2016.10.046.

References

[1] E. Meng, R. Sheybani, Lab Chip 14 (2014) 3233–3240.
[2] B.C.-K. Tee, A. Chortos, A. Berndt, A.K. Nguyen, A. Tom, A. McGuire, Z.C. Lin, K. Tien, W.-G. Bae, H. Wang, Science 350 (2015) 313–316.
[3] Y. Yang, H. Zhang, Z.-H. Lin, Y.S. Zhou, Q. Jing, Y. Su, J. Yang, J. Chen, C. Hu, Z.L. Wang, ACS Nano 7 (2013) 9213–9222.
[4] S. Park, H. Kim, M. Vosgueritchian, S. Cheon, H. Kim, J.H. Koo, T.R. Kim, S. Lee, G. Schwartz, H. Chang, Adv. Mater. 26 (2014) 7324–7332.
[5] B. Meng, W. Tang, Z.-h. Too, X. Zhang, M. Han, W. Liu, H. Zhang, Energy Environ. Sci. 6 (2013) 3235–3240.
[6] D.J. Lipomi, M. Vosgueritchian, B.C. Tee, S.L. Hellstrom, J.A. Lee, C.H. Fox, Z. Bao, Nat. Nanotechnol. 6 (2011) 788–792.
[7] P. Bai, G. Zhu, Q. Jing, J. Yang, J. Chen, Y. Su, J. Ma, G. Zhang, Z.L. Wang, Adv. Funct. Mater. 24 (2014) 5807–5813.
[8] W. Seung, M.K. Gupta, K.Y. Lee, K.-S. Shin, J.-H. Lee, T.Y. Kim, S. Kim, J. Lin, J.H. Kim, S.-W. Kim, ACS Nano 9 (2015) 3501–3509.
[9] G. Schwartz, B.C.-K. Tee, J. Mei, A.L. Appleton, D.H. Kim, H. Wang, Z. Bao, Nat. Commun. 4 (2013) 1859.
[10] S.C. Mannsfeld, B.C. Tee, R.M. Stoltenberg, C.V.H. Chen, S. Barman, B.V. Muir, A.N. Sokolov, C. Reese, Z. Bao, Nat. Mater. 9 (2010) 859–864.
[11] N. Lu, C. Lu, S. Yang, J. Rogers, Adv. Funct. Mater. 22 (2012) 4044–4050.
[12] C. Wang, D. Hwang, Z. Yu, K. Takei, J. Park, T. Chen, B. Ma, A. Javey, Nat. Mater. 12 (2013) 899–904.
[13] C.L. Choong, M.B. Shim, B.S. Lee, S. Jeon, D.S. Ko, T.H. Kang, J. Bae, S.H. Lee, K.E. Byun, J. Im, Adv. Mater. 26 (2014) 3451–3458.
[14] D. Kang, P.V. Pikhitsa, Y.W. Choi, C. Lee, S.S. Shin, L. Piao, B. Park, K.-Y. Suh, T.-i. Kim, M. Choi, Nature 516 (2014) 222–226.
[15] L.Y. Chen, B.C.-K. Tee, A.L. Chortos, G. Schwartz, V. Tse, D.J. Lipomi, H.-S.P. Wong, M.V. McConnell, Z. Bao, Nat. Commun. 5 (2014).
[16] T. Someya, T. Sekitani, S. Iba, Y. Kato, H. Kawaguchi, T. Sakurai, Proc. Natl. Acad. Sci. USA 101 (2004) 9966–9970.
[17] B. Mosadegh, P. Polygerinos, C. Keplinger, S. Wennstedt, R.F. Shepherd, U. Gupta, J. Shim, K. Bertoldi, C.J. Walsh, G.M. Whitesides, Adv. Funct. Mater. 24 (2014) 2163–2170.
[18] C. Yan, J. Wang, W. Kang, M. Cui, X. Wang, C.Y. Foo, K.J. Chee, P.S. Lee, Adv. Mater. 26 (2014) 2022–2027.
[19] Y. Wang, L. Wang, T. Yang, X. Li, X. Zang, M. Zhu, K. Wang, D. Wu, H. Zhu, Adv. Funct. Mater. 24 (2014) 4666–4670.
[20] L. Dhakar, P. Pitchappa, F.E.H. Tay, C. Lee, Nano Energy 19 (2016) 532–540.
[21] L. Pan, A. Chortos, G. Yu, Y. Wang, S. Isaacson, R. Allen, Y. Shi, R. Dauskardt, Z. Bao, Nat. Commun. 5 (2014).
[22] S. Gong, W. Schwalb, Y. Wang, Y. Chen, Y. Tang, J. Si, B. Shirinzadeh, W. Cheng, Nat. Commun. 5 (2014).
[23] T. Yamada, Y. Hayamizu, Y. Yamamoto, Y. Yomogida, A. Izadi-Najafabadi, D.N. Futaba, K. Hata, Nat. Nanotechnol. 6 (2011) 296–301.
[24] M. Park, H. Kim, J.P. Youngblood, Nanotechnology 19 (2008) 055705.
[25] Y. Zang, F. Zhang, D. Huang, X. Gao, C.-a. Di, D. Zhu, Nat. Commun. 6 (2015).
[26] D.J. Lipomi, M. Vosgueritchian, B.C. Tee, S.L. Hellstrom, J.A. Lee, C.H. Fox, Z. Bao, Nat. Nanotechnol. 6 (2011) 788–792.
[27] D.J. Lipomi, M. Vosgueritchian, B.C. Tee, S.L. Hellstrom, J.A. Lee, C.H. Fox, Z. Bao, Nat. Nanotechnol. 6 (2011) 788–792.
[28] R.-Z. Li, A. Hu, T. Zhang, K.D. Oakes, ACS Appl. Mater. Interfaces 6 (2014) 21721–21729.
[29] C. Pan, L. Dong, G. Zhu, S. Niu, R. Yu, Q. Yang, Y. Liu, Z.L. Wang, Nat. Photonics 7 (2013) 752–758.
[30] K.I. Park, J.H. Son, G.T. Hwang, C.K. Jeong, J. Ryu, M. Koo, I. Choi, S.H. Lee, M. Byun, Z.L. Wang, Adv. Mater. 26 (2014) 2514–2520.
[31] L. Persano, C. Dagdeviren, Y. Su, Y. Zhang, S. Girardo, D. Pisignano, Y. Huang, J.A. Rogers, Nat. Commun. 4 (2013) 1633.
[32] Z. Pi, J. Zhang, C. Wen, Z.-b. Zhang, D. Wu, Nano Energy 7 (2014) 33–41.
[33] F.-R. Fan, L. Lin, G. Zhu, W. Wu, R. Zhang, Z.L. Wang, Nano Lett. 12 (2012) 3109–3114.
[34] G. Zhu, W.Q. Yang, T. Zhang, Q. Jing, J. Chen, Y.S. Zhou, P. Bai, Z.L. Wang, Nano

Lett. 14 (2014) 3208–3213.
[35] L. Lin, Y. Xie, S. Wang, W. Wu, S. Niu, X. Wen, Z.L. Wang, ACS Nano 7 (2013) 8266–8274.
[36] H. Wang, Z. Xiang, P. Giorgia, X. Mu, Y. Yang, Z.L. Wang, C. Lee, Nano Energy 23 (2016) 80–88.
[37] Q. Shi, T. Wang, T. Kobayashi, C. Lee, Appl. Phys. Lett. 108 (2016) 193902.
[38] Q. Shi, T. Wang, C. Lee, Sci. Rep. 6 (2016).
[39] L. Zhao, Q. Zheng, H. Ouyang, H. Li, L. Yan, B. Shi, Z. Li, Nano Energy 28 (2016) 172–178.
[40] X. Wang, Z.L. Wang, Y. Yang, Nano Energy 26 (2016) 164–171.
[41] H.-J. Choi, J.H. Lee, J. Jun, T.Y. Kim, S.-W. Kim, H. Lee, Nano Energy 27 (2016) 595–601.
[42] Q. Zheng, H. Zhang, B. Shi, X. Xue, Z. Liu, Y. Jin, Y. Ma, Y. Zou, X. Wang, Z. An, ACS Nano (2016).
[43] B. Shi, Q. Zheng, W. Jiang, L. Yan, X. Wang, H. Liu, Y. Yao, Z. Li, Z.L. Wang, Adv. Mater. 28 (2016) 846–852.
[44] Q. Zheng, B. Shi, F. Fan, X. Wang, L. Yan, W. Yuan, S. Wang, H. Liu, Z. Li, Z.L. Wang, Adv. Mater. 26 (2014) 5851–5856.
[45] Q. Zheng, Y. Jin, Z. Liu, H. Ouyang, H. Li, B. Shi, W. Jiang, H. Zhang, Z. Li, Z.L. Wang, ACS Appl. Mater. Interfaces (2016).
[46] K.Y. Lee, M.K. Gupta, S.-W. Kim, Nano Energy 14 (2015) 139–160.
[47] J. Chun, J.W. Kim, W.-s. Jung, C.-Y. Kang, S.-W. Kim, Z.L. Wang, J.M. Baik, Energy Environ. Sci. 8 (2015) 3006–3012.
[48] Z.L. Wang, ACS Nano 7 (2013) 9533–9557.
[49] S. Wang, L. Lin, Z.L. Wang, Nano Energy 11 (2015) 436–462.
[50] J.C. Yeo, J. Yu, M. Shang, K.P. Loh, C.T. Lim, Small (2016).
[51] J.C. Yeo, J. Yu, Z.M. Koh, Z. Wang, C.T. Lim, Lab Chip 16 (2016) 3244–3250.
[52] Z.H. Lin, G. Cheng, L. Lin, S. Lee, Z.L. Wang, Angew. Chem. Int. Ed. 52 (2013) 12545–12549.
[53] S.-B. Jeon, D. Kim, M.-L. Seol, S.-J. Park, Y.-K. Choi, Nano Energy 17 (2015) 82–90.
[54] S.B. Jeon, M.L. Seol, D. Kim, S.J. Park, Y.K. Choi, Adv. Electron. Mater. (2016).
[55] X. Li, M.-H. Yeh, Z.-H. Lin, H. Guo, P.-K. Yang, J. Wang, S. Wang, R. Yu, T. Zhang, Z.L. Wang, ACS Nano 9 (2015) 11056–11063.
[56] L. Zheng, Z.-H. Lin, G. Cheng, W. Wu, X. Wen, S. Lee, Z.L. Wang, Nano Energy 9 (2014) 291–300.
[57] Z.H. Lin, G. Cheng, S. Lee, K.C. Pradel, Z.L. Wang, Adv. Mater. 26 (2014) 4690–4696.
[58] Z.-H. Lin, G. Cheng, W. Wu, K.C. Pradel, Z.L. Wang, ACS Nano 8 (2014) 6440–6448.
[59] G. Zhu, Y. Su, P. Bai, J. Chen, Q. Jing, W. Yang, Z.L. Wang, ACS Nano 8 (2014) 6031–6037.
[60] X.J. Zhao, G. Zhu, Y.J. Fan, H.Y. Li, Z.L. Wang, ACS Nano 9 (2015) 7671–7677.
[61] D. Choi, S. Lee, S.M. Park, H. Cho, W. Hwang, D.S. Kim, Nano Res. (8) (2015) 2481–2491.
[62] W. Tang, T. Jiang, F.R. Fan, A.F. Yu, C. Zhang, X. Cao, Z.L. Wang, Adv. Funct. Mater. 25 (2015) 3718–3725.
[63] T. Kim, J. Chung, D.Y. Kim, J.H. Moon, S. Lee, M. Cho, S.H. Lee, S. Lee, Nano Energy 27 (2016) 340–351.
[64] H. Chen, Y. Song, M. Han, B. Yu, X. Cheng, X. Chen, D. Chen, H. Zhang, in: Proceedings of the IEEE 29th International Conference on Micro Electro Mechanical Systems (MEMS), 2016, pp. 1252–1255
[65] M. Han, B. Yu, G. Qiu, H. Chen, Z. Su, M. Shi, B. Meng, X. Cheng, H. Zhang, J. Mater. Chem. A 3 (2015) 7382–7388.